International Journal of Latest Engineering and Management Research (IJLEMR)
ISSN: 2455-4847
www.ijlemr.com || Volume 08 – Issue 05 || May 2023 || PP. 70-84

3-D Numerical simulation of mining-induced dynamic failure and energy release mechanism of entry roof

Xiaokang Wang*
[1](*School of Energy Science and Engineering, Henan Polytechnic University, Jiaozuo, 454003, China)*

Abstract: Dynamic impact of entry roof is a widespread and serious dynamic damage problem in deep underground engineering. In this study, the displacement back analysis method based on numerical modeling and field observations is conducted to investigate the underlying dynamic impact mechanism of entry roof. A Mohr-Coulomb strain softening model is adopted to describe the energy release characteristics of rock mass, and the initial mechanical values of rock mass are estimated by the Geological Strength Index (GSI) system. A back-analysis algorithm for optimizing mechanical values of rock mass is proposed and implemented with ABAQUS, and a static and dynamic coupling analysis approach is developed for longwall mining simulation based on the "Dynamic/Implicit" solving mode. The variations of the acceleration distribution in main roof, the strain energy release process in barrier coal pillar and the mining-induced stress evolution during longwall mining process are obtained and analyzed. The mechanism of the entry roof shock in the under-gob mining situation is inferred and explained based on the numerical simulation results and the overlying strata structure theory. The displacement back analysis method shows excellence performance and feasibility to determine the mechanical parameter values for rock mass and reappear the entry roof shock phenomenon. The entry roof shock accident is very correlated with the strain energy release of the barrier coal pillar, indicating that the instantaneous instability of coal pillar triggers the entry roof shock accident. Affected by the under-gob mining activity, the fractured main key hard strata slip, causing the V-shaped strata blocks above the coal pillar in the upper coal seam to suddenly fall over and generating a dynamic impact onto the coal pillar in the lower coal seam. Subjected to the static-dynamic coupling load, the coal pillar in the under-gob panel bursts and collapses with the entry roof shocking and subsiding.

Keywords: displacement back analysis; entry roof shock; coal burst; strain energy release; under-gob longwall mining

1. Introduction

Rock burst and rock roof shock are serious mining safety problems in many countries in recent half a century [1][2]. Coal pillar burst (a kind of rock burst) and entry roof shock at longwall panel in coal mine usually induce a sudden release of elastic energy accumulated in coal-rock mass around the entry, which causes serious damage to the supports, even ground surface subsidence and local earthquakes [3]. In 1997, a 3.9-magnitude quake happened in Crandall Canyon coal mine in Utah state, US, which was induced by a coal pillar burst[4][5]. China is the largest coal production country, in which coal bursts are regarded as the greatest hidden danger for more than 140 coal mines [6]. There are more than 600 coal burst events occurred and caused more than 300 fatal injuries from 2006 to 2013 [7]. It is reported that more than 85% of coal bursts happen around the gateroad in longwall panel, especially in the gob-side entry [8][9][10].

Analysis of the coal burst mechanism, prediction and assessing of coal burst are significant premises for future targeted prevention [11]. Many researchers studied the coal burst mechanism of longwall mining by field micro-seismic monitoring, numerical simulation, and rock mechanics experiments in the past 60 years. A variety of hypotheses about rock burst (or coal burst), such as the energy release theory [12], the system stiffness theory [13], the static and dynamic strength theory [14], the fold catastrophe theory [15] and the deformation instability theory [16] were proposed. Jiang et al. [17][18] classified the coal bursts into three categories according to the geological conditions: coal material failure, coal burst induced by hard roof and induced by tectonic structures. He et al. [19] analyzed the critical damage factor of coal and suggested that the high static stress environment provides high strain energy for coal sudden failure, and the dynamic impact mainly induces sudden failure of coal-rock under high static loads. Dou et al. [20] and Li et al.[21]put forward a stress concentration theory for explaining coal burst, in which an over-stress state is generated from a combination of static and dynamic load concentration. The dynamic stress concentration is formed by the sudden collapse of the hard and thick overhanging strata, which generates a shock wave onto coal pillars.

In China northwest coal mines, the longwall mining parameters, especially the working face length, the mining advancing speed and the mining height, become greater over the past 10 years due to the good geological conditions and the high-level mining mechanization and automation technology [22]. The high-intensity mining activity causes new problems of mining-induced pressure appearances and dynamic disasters,

especially the under-gob coal pillar burst and entry roof shock. According to the coal industry regulations in China and the economic mining experiences, in general, if a coal mine has two coal seams and the distance between the two coal seams is relative far (e.g. more than 30 m), the upper coal seam should be extracted before the lower coal seam mining. Therefore, the rock roofs above the upper coal seam undergo twice effects of mining activities. After the upper coal seam is mined by longwall mining method, a lot of gobs are generated, and the overlying strata will fracture, move down, and form discontinuous roof structures. When mining in lower coal seam, the balance state of the upper coal seam roof structures will be broken and changed to reach a new balance state. During this process, the reactivation of the upper coal seam roof structures, such as sudden collapse, plays a significant role in affecting the stability and stress distribution of the lower coal seam roofs. Consequently, it is of importance to study the under-gob mining-induced roof movement, energy release and the mechanism of lower coal seam roof shock.

Numerical simulation is a good way to reappear entry shock accident and study its mechanism. However, it is usually difficult to evaluate and determine the mechanical model and parameter values for describing the deformation behavior and energy release characteristics of rock mass. The mechanical property of rock samples tested in laboratory cannot directly used in numerical simulation of underground mining because of the large difference between rock samples and the jointed rock mass [23]. Hoek et al.[24][25][26]proposed the GSI (Geological strength index) system for rock mass parameter determination. The GSI value of rock mass can be quantified based on RQD (Rock Quality Designation) method, RMQ (Rock Mass Quality) method, RMR (Rock Mass Rate) or RMi (Rock Mass index) method[27]. The mechanical values of rock mass determined by GSI system usually are close to the real values of rock mass at engineering scale, but there may still be some errors, which make the mechanical behavior and deformation behavior of rock mass can not be satisfied at the same time. Subsequently, Hoek and Brown [28] pointed out that the mechanical values of rock mass determined by GSI system should better be adjusted by computer back analysis. That is also important for modeling the coal burst and entry roof shock problems which is accompanied by strain energy release. For numerical simulation of strain energy release, the deformation and strength behaviors of rock (or coal) mass are very critical for calculating the strain energy density which is the integration of stress on displacement. Essentially, the transformation methods of geological body mechanical property between different scales, such as the GSI system, back analysis [29], fractal theory [30], can be regarded as the renormalization method [31] in Quantum Field theory which is used to find fixed points of scale transformation.

In this study, the displacement back analysis method based on numerical modeling and field observations of surface subsidence is conducted to investigate the entry roof shock accident and the coal pillar burst at longwall panel No. 42105 in Buertai coal mine. A Mohr-Coulomb strain softening model is adopted to describe the energy release characteristics of rock mass, and those initial mechanical values of rock mass are determined by laboratory test results and GSI system. A back-analysis algorithm for adjusting the mechanical values of rock mass is proposed and implemented with ABAQUS, and a static and dynamic coupling analysis approach is developed for longwall mining simulation based on the "Dynamic/Implicit" solving mode in ABAQUS. The variations of the acceleration distribution in main roof, the strain energy release process in barrier coal pillar and the mining-induced stress evolution during longwall mining process are obtained and analyzed. Finally, based on the numerical simulation results and the overlying strata structure theory, the mechanism of the entry roof shock in the under-gob mining situation is inferred and explained. By presenting a complete case of back analysis, this study is of significance to develop the application of displacement back analysis in underground longwall mining-induced accident investigation and deepen the understanding of entry roof shock mechanism induced by mining under gobs.

2. Field investigations on entry roof shock

Buertai coal mine of the Shendong Coal Mining Group is located in Erdos basin in Inner Mongolia province, China. It is a typical coal mine with large mining parameters and multiple coal seams, of which it produces 20 M tons per annum using longwall mining method, the longwall mining advancing speed reaches 18 m/d, the length of working face is more than 230 m, and the average mining height is 6.02 m. Buertai coal mine has two flat coal seams. The upper and the lower coal seams are numbered as No. 22 and No. 42 respectively, as shown in Fig. 1. Coal seam No. 22 was extracted before coal seam No. 42. The average thicknesses of coal seams No. 22 and No. 42 are 3.12 m and 6.02 m, respectively. Coal seam No. 42 mainly is hard coal, and its average uniaxial compression strength tested by coal samples is 31.2 MPa. The strata between the two coal seams mainly are fine sandstone and sandy mudstone (Fig. 1(b)). The average distance between the two seams is 61.81 m. The average depths of coal seams No. 22 and No. 42 are 324.14 m and 391.97 m respectively.

As shown in Fig. 2(a), the entry roof shock accident happened around the gob-side entry (named No. 42105-G) in longwall panel No. 42105 in Buertai coal mine. The panel No. 42105 is in the side of the gob No. 42104, and is under the gobs No. 22104 and No. 22015. The panel No. 42105 is 230 m in working face length

and 5200 m in mining advancing direction. The width of the coal pillar No. 42 which is between the panels No. 42105 and No. 42104 is 30 m. The widths of the coal pillars between the gobs No. 22013 and No. 22104 (named No. 22) and between the gobs No. 22104 and No. 22105 are 80 m and 20 m, respectively.

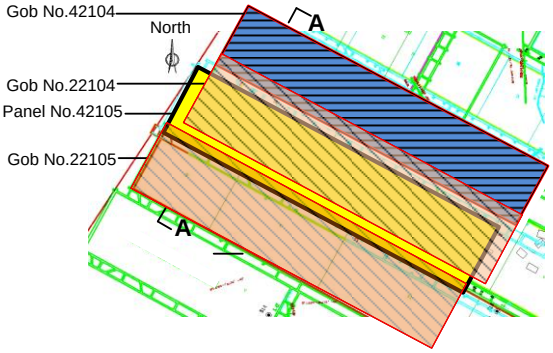

(a)

Column	Coal seam	Accumulating depth/m	Thickness/m	Rock type
		321.02	11.79	Sandy mudstone
	No.22	324.14	3.12	Coal
		329.44	5.30	Sandy mudstone
	22-b	330.07	0.63	Coal
		338.39	8.32	Fine sandstone
		353.40	15.01	Sandy mudstone
		371.42	18.02	Fine sandstone
		385.95	14.53	Sandy mudstone
	No.42	391.97	6.02	Coal
		423.30	10.79	Sandy mudstone

(b)

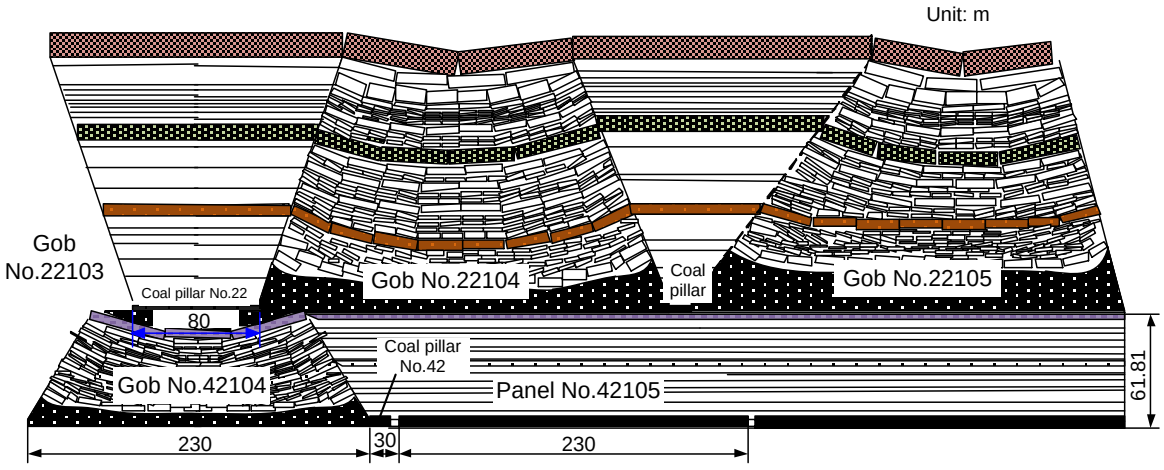

(c)

Fig. 1 The location of longwall panel No. 42105 and the rock layer distribution between coal seams No. 22 and No. 42 in Buertai coal mine; (a) the top view of longwall panels; (b) the rock layer distribution between coal seams No. 22 and No. 42; and (c) the sectional drawing along A-A in (a).

Fig. 2 shows the location of the roof shock accident and the hydraulic single props break situation at the accident site. When working face No. 42105 advanced about 239.75 m, a roof shock happened in 10-60 m ahead of the working face in the entry No. 42105-G. More than 120 hydraulic single props were bent or broken off, and fell down instantly with a huge roar coming from the roof (Fig. 2(b) and (c)).

After this shock phenomenon, it was found that the coal pillar No. 42 behind the longwall working face (B zone in Fig. 2(a)) bloated and bumped about 0.5-1.3 m, as shown in Fig. 2(d). This fact indicates that the entry roof shock may be correlated with the coal pillar failure.

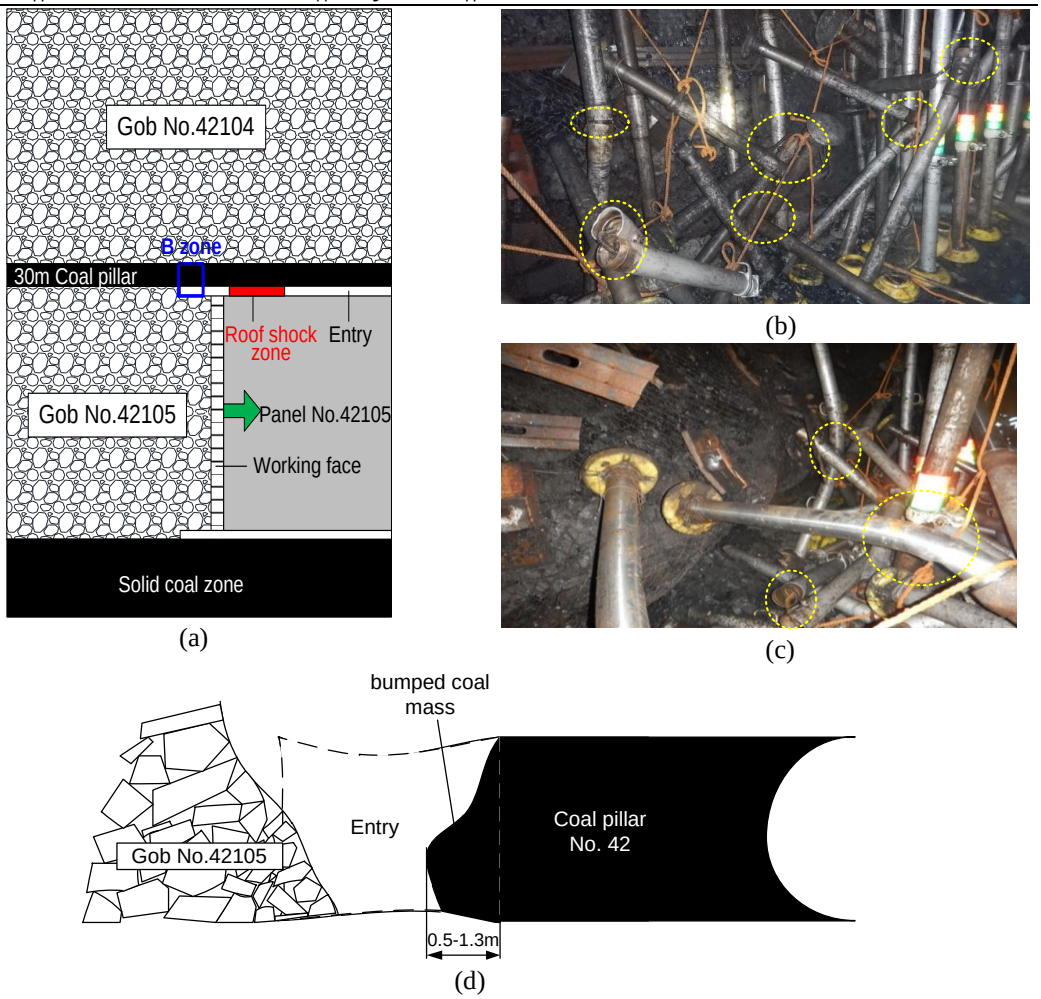

Fig. 2 (a) the location of the entry roof shock in a top view; (b) and (c) the photos of failure situation of hydraulic single props in the roof shock zone; (d) a schematic of bump of coal pillar No. 42 at B zone shown in (a).

3. Numerical simulation procedures

3.1 Numerical model

A 3-D numerical model is created by ABAQUS, as shown in Fig. 3. In fact, the lengths in mining advancing direction are more than 5000 m for those longwall panels, but it has to be shortened as 800 m to make sure that the entry roof shock place is in the middle of the model and to reduce the computation complexity in the 3-D numerical model. Thus, the 3-D numerical model is 970 m in width, 1200 m in length (the mining advancing direction) and 430 m in height. The top face of this model is flat and ignore the landform because the altitude of the ground surface above panels No. 42014 and No. 42105 varies from +1370 m to +1380 m. This 3-D model is meshed into about 930,000 C3D8 elements. The C3D8 element is a 3-D 8-node linear brick element with 4 integration points. The boundary conditions without reflection are set around and at the bottom of the model by the infinite element method in ABAQUS.

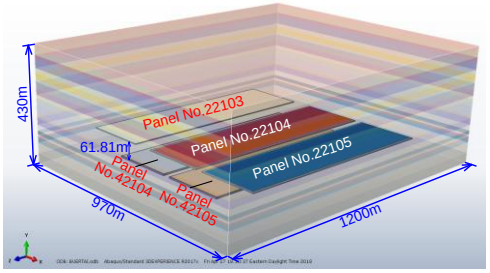

Fig. 3 The 3-D numerical model created by ABAQUS

3.2 Mechanical models of rock layer, interface and gob

3.2.1 Rock layer mechanical model

Roof shock question involves the strain energy release process and energy transfer from elastic energy to kinetic energy. The elastic energy in solid finite element is calculated based on stress and strain components. Therefore, it is crucial to choose a relative accurate model to describe the energy release characteristics for simulating roof shock phenomenon. Moreover, for the displacement back analysis process, the final output parameter values are evaluated and determined by field observation data and numerical simulation results, thus, the rock deformation behavior should also be considered seriously in the numerical simulation.

The initial mechanical parameter values of rock layers are listed in Table. 1 In table. 1, the rock layers with ID of 4, 8, 12, 14 and 20 are relatively hard and thick. According to literature [32], the dilation angle can be assigned as 1/3-1/2 of the value of friction angle. The *E* of the loess refers to its deformation modulus. In ABAQUS, the strain softening functions, $c(\varepsilon_p)$, $\varphi(\varepsilon_p)$ and $\delta_\tau(\varepsilon_p)$, are defined as table functions of ε_p (Dassault Systemes Simulia Corporation.2014). c and φ are linearly reduced with increasing the plastic strain. When the plastic strain reaches 5×10^{-3}, c and φ decrease by 75%. The decrease slopes of c and φ are modified by the displacement back analysis. After 5×10^{-3}, c and φ remain unchanged as the 25% of their initial values to describe the rock's residual strength.

Table 1 Initial parameter values of rock layers

Rock layer ID	Type	ρ /kg/m^3	E/GPa	v	φ/°	c/MPa	ψ /°	δ_t /MPa
1	Loess	1642	2.8	0.42	18.00	0.003	8	0.0035
2	Fine Sandstone	2622	1.1	0.28	30.50	6.04	12	0.42
3	Sandy mudstone	2511	2.2	0.25	26.70	8.28	9	1.11
4	Mid-grain sandstone	2650	9.6	0.27	32.36	7.92	10	4.24
5	Coarse sandstone	2482	0.7	0.25	32.60	3.96	12	0.10
6	Sandy mudstone	2565	1.5	0.22	21.80	18.06	9	1.70
7	Coarse sandstone	2503	1.2	0.27	25.09	6.87	12	0.62
8	Sandy mudstone	2418	8.9	0.31	25.86	16.99	10	3.20
9	Mid-grain sandstone	2387	4.6	0.28	32.36	5.81	12	1.06
10	Siltite	2531	7.2	0.26	30.85	8.72	10	0.77
11	Fine Sandstone	2575	1.2	0.26	21.02	6.24	8	0.49
12	Mid-grain sandstone	2486	4.9	0.24	32.36	6.05	12	3.50
13	Sandy mudstone	2323	4.8	0.24	24.28	14.96	9	2.24
14	Siltite	2439	11.7	0.29	27.67	10.60	10	2.55
15	Coarse sandstone	2276	1.4	0.26	34.23	3.31	12	1.82
16	Sandy mudstone	2547	6.5	0.26	26.40	8.76	10	1.31
17	No.22 coal	1348	1.1	0.24	26.84	2.26	11	0.8
18	Sandy mudstone	2466	4.0	0.25	24.90	8.72	10	1.61
19	Fine Sandstone	2490	3.2	0.26	30.10	6.42	13	2.82
20	Sandy mudstone	2427	7.1	0.25	33.70	16.10	12	3.76
21	Fine Sandstone	2533	5.0	0.25	31.50	4.76	14	1.34
22	Sandy mudstone	2442	5.3	0.26	31.80	4.63	13	1.88
23	No.42 coal	1372	2.2	0.25	31.00	13.6	12	1.4
24	Fine Sandstone	2605	6.1	0.26	20.18	26.91	9	4.61

3.2.2 Mechanical model of rock layer interface

The Coulomb friction model is adopted to represent the tangential behavior of rock layer interfaces in ABAQUS, as shown in Fig. 4. The interface normal behavior is assumed as hard contact with an initial tensile strength. The interface shear stiffness is calculated by a penalty method, as a result, ABAQUS has to allow a very small elastic slip distance which is less than 0.05% of the element characteristic length when the interface shear stress is lower than shear strength [33]. Generally, the tensile strength of rock layer interface is significantly weaker than that of rock, and is difficult to be measured exactly in laboratory or in situ. The initial tensile strength is set as 0.01 MPa, and the initial friction coefficient, □, is assigned as 0.30.

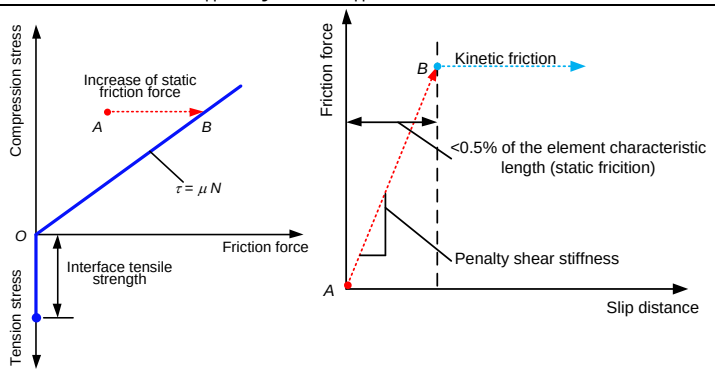

(a) (b)

Fig. 4 The mechanical model of rock layer interface;(a) the tension and friction models;(b) the schematic of penalty shear stiffness and micro-slip in static friction stage.

3.2.3 Gob compression model

The gob compaction process should be considered in longwall mining simulation, which significantly affects the overlying rock layer subsidence. The gob compression model adopted in this study is proposed by Salamon in 1991 [34]. In this model, the vertical stress ε_v in the gob increases with the vertical strain ε_v increases, according to the equation:

$$\sigma_v = \frac{E_{gob}\varepsilon_v}{\varepsilon_{gob} - \varepsilon_v} \tag{1}$$

Where E_{gob} is the gob initial deformation modulus, ε_{gob} is the limiting vertical strain.

The initial values for the two parameters are assigned as E_{gob} =3.5 MPa and ε_{gob} =0.5 [35]. The gob is simulated as non-linear elastic materials to describe its gradual compaction feature by implementing Equation (21) into ABAQUS. The gob bulk modulus is continually increased as a function of ε_v within the gob space. For each 3D solid element in the gob, the bulk modulus, *K*, can be obtained by [36]:

$$K = \frac{1.75}{0.5 - \varepsilon_z} \tag{2}$$

Where ε_z is the vertical strain component of the element in the gob zone.

With longwall working face advancing, the caving zone, fractured zone and continuous deformation zone are generated above the coal seam, as shown in Fig. 5. The height of the caving zone decreases as the caved rocks filled in gob are gradually compressed. Therefore, the initial height of the gob zone is determined by the initial height of caving zone. According to the official investigation in China, the final compressed height of caving zone can be calculated as:

$$h_c^f = \frac{100M}{2.1M + 16} \pm 2.5 \tag{3}$$

Where h_c^f is the final compressed height of caving zone, m; *M* is the coal mining height, 6.02 m for Buertai coal mine. According to Equation (23), the final compressed height of caving zone is from 18.52 m to 23.52 m for Buertai coal mine.

The expansion factor of the caving zone can be defined as:

$$k_c = \frac{H_c}{H_r} \tag{4}$$

Where k_c is the expansion factor of the caving zone; H_c is caving zone height, m; H_r is the total thickness of the immediate roof layers before caving, m.

With the caving zone being compressed, the expansion factor k_c of the caving zone decreases. It is assumed that the initial and the final expansion factor of the caving zone are 1.25(k_c^i) and 1.05(k_c^f), respectively.

The initial gob height (i.e. the height of gob zone) h_c^i can be calculated by:

$$h_c^i = \frac{k_c^i}{k_c^f} h_c^f \tag{5}$$

According to Equation (25), h_c^i is from 22.05m to 28m. In this study, the initial gob height is finally assigned as 25 m.

This gob deformation behavior is updated by implementing a user material subroutine USDFLD by programming language "Fortran" in ABAQUS.

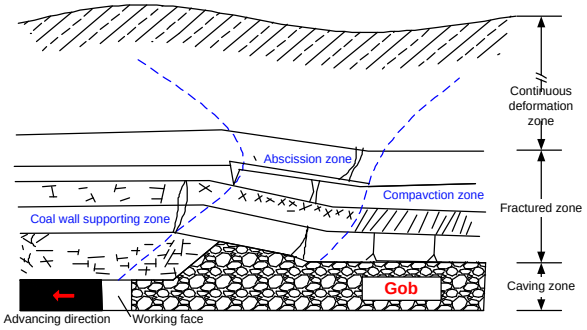

Fig. 5 Schematic of caving zone and gob zone for longwall panel

3.3 Simulation technique of mining-induced intense shock

The "Dynamic/Implicit" solving mode, which uses the "standard" solver in ABAQUS, is adopted to simulate the longwall mining process. The "Dynamic/Implicit" solving method is suitable for simulating longwall mining processes due to its advantages of good convergence, and static and dynamic coupling analysis [33]. In each longwall mining cycle, the excavation of coal mass is implemented as a quasi-static process to obtain the stress and failure state of all elements, then the dynamic analysis will be implemented to calculate the softening behavior of those previous critical failure state elements and the strain energy release process, as shown in Fig. 6.

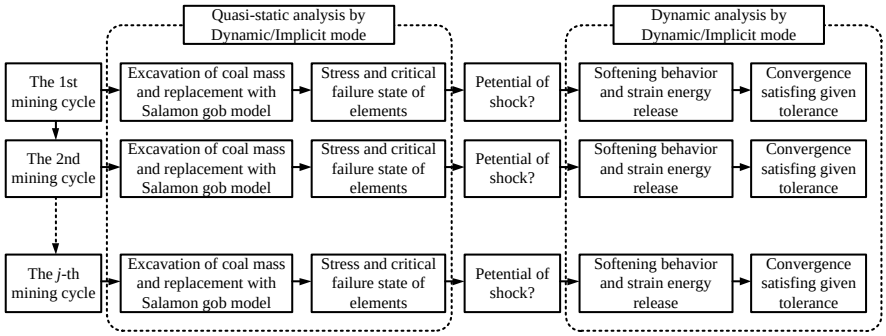

Fig. 6 Static-dynamic coupling solving technique for simulating intense shock problem

The matrix storage type of finite element equations is unsymmetric. The solution technique is full newton method. A viscosity coefficient of the C3D8 element is set to 0.0001 to improve the non-linear analysis convergence. According to ABAQUS documentation, the coefficient of critical numerical damping for rock mass falls into 2%-5%, so the critical damping value is set as 5% [33].

The longwall panels No. 22013, No. 22104, No. 22105, No. 42104 and No. 42105 are mined sequentially. The stress distribution in an elastic body is irrelevant with the loading or unloading paths, but the stress and strain evolution in plastic body are significantly affected by the loading and unloading paths. Therefore, the failure and deformation of the roof strata are influenced by the mining sequence, and it is essential to implement the mining process in ABAQUS as the real mining process in coal mine as far as possible. Fig. 7 shows one typical cycle in the numerical mining process. The advancing distance in each mining cycle should be less than the main roof fracturing distance of 12 m to 32 m to avoid its influences on the fracture behavior and pressure variation characteristics of the main roof. Consequently, the mining step length for one cycle is set to 5 m; videlicet, the material property of gob zone is transferred to Salamon model at a speed of 5 m/cycle.

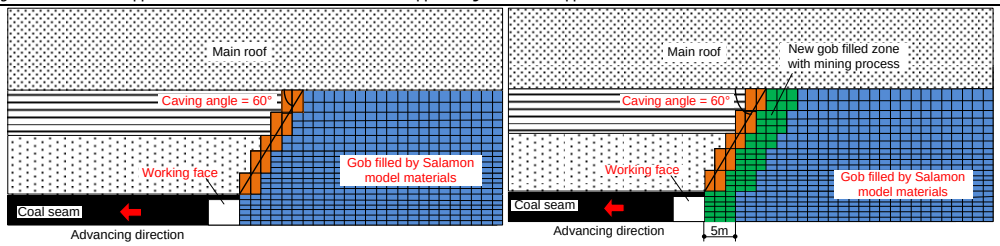

(a) (b)

Fig. 7 Schematic of the numerical longwall mining process in one cycle;(a) before this mining cycle; (b) after new gob is filled with Salamon model materials.

4. Numerical simulation results and analysis

4.1 Ground surface subsidence result

There are two perpendicular observation lines arranged in the ground surface area above the longwall panels No. 42104 and No. 42105, as shown in Fig. 8. Line A, on which there are 49 monitoring points numbered from A1 to A49, is parallel to the mining advancing direction, and is in the middle of the surface area mapped by panel No. 42105. Line B including 30 monitoring points numbered from B1 to B30 is perpendicular to the mining advancing direction. The horizontal distance between line B and the open-off cut of panel No. 42105 is about 610 m.

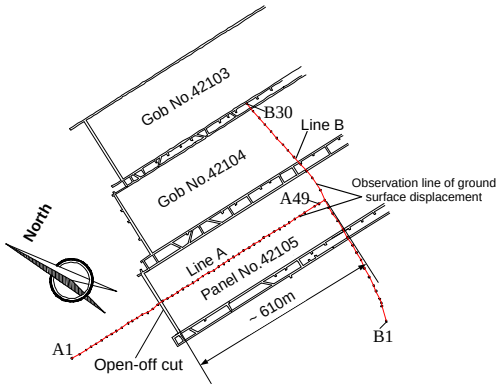

Fig. 8 The observation lines arrangement for ground surface displacement observations

The final displacement results calculated by displacement back analysis method compared to the field observation data are plotted in Fig. 9. Fig. 9(a) and (b) are results for line A and line B, respectively. Through the back analysis, the numerical subsidence values are close to the field observation results, which indicates the final mechanical parameter values of the strata and gob are accurate enough to represent the underground materials. The simulation results of the entry roof shock using the final parameter values are discussed in Section 5.2-5.4.

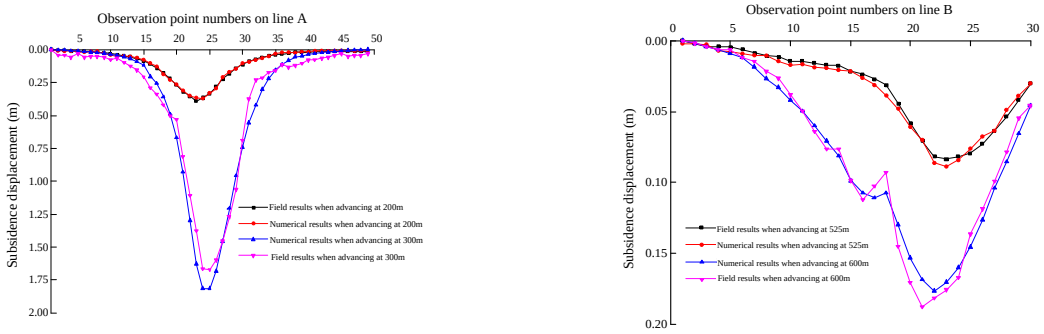

(a) (b)

Fig. 9 The final surface subsidence displacement calculated by displacement back analysis;(a) line A; (b) line B

4.2 The roof layer impact characteristics

The stress concentration factor and the energy accumulation degree [37] are widely used to evaluate rock burst risks and predict rock burst. However, those two indexes cannot represent and describe the intensity of

rock impact phenomenon. The strain energy in rock mass is dissipated and released as plastic deformation energy, fracture energy for crack propagation and kinetic energy for inducing rock burst or rock shock [38]. Usually, the impact and shock happen instantaneously, which implies the energy transferring rate from strain energy to kinetic energy is extremely fast. The kinetic energy release speed is adopted to reflect and assess whether the roof shock is happening.

For a rock micro unit dV, the kinetic energy converted from strain energy is defined as:

$$\Delta E_k = \frac{1}{2}\rho_m \Delta(v_m^2)\mathrm{d}V \tag{6}$$

Where ρ_m is rock density, kg/m^3; Δv_m is the velocity increment of the rock micro unit, m/s.

It is assumed that the rock micro unit is subjected to a constant resultant force inducing energy conversion in a very short period Δt. According to the Newton's second law, its acceleration is also constant in Δt. Consequently, the kinetic energy release speed $f(t)$ can be calculated as:

$$f(t) = \lim_{\Delta t \to 0} \Delta E_k / \Delta t = \frac{1}{2}\rho_m \mathrm{d}V \lim_{\Delta t \to 0}[\Delta(v_m^2)/\Delta t] = \rho_m \mathrm{d}V a^2 t \tag{7}$$

Where t is time, s; a is the acceleration of the rock micro unit, m/s^2. According to Equation (27), the acceleration a can be an index to represent the impact intensity and to describe the roof shock appearance.

Fig. 10(a), (b) and (c) are the acceleration contour section maps at working face No. 42105 when working face No. 42105 advances at 235 m, 240 m and 245 m, respectively. The acceleration distribution along with the mining advancing direction in the main roof which is 60 m above the entry No. 42105-G is drawn in Fig. 11. From Fig. 10 and 11, the maximum acceleration values of the main roof when working face No. 42105 advances at 235 m and 245 m are less than 10 m/s^2, whereas the max acceleration when advancing at 240 m reaches 65.7 m/s^2, which is greater dramatically than it at 235 m and 245 m. This result indicates that the roof shock event is reappeared by numerical simulation successfully, and implies that the mechanical parameter values calculated by the displacement back analysis method are exact enough.

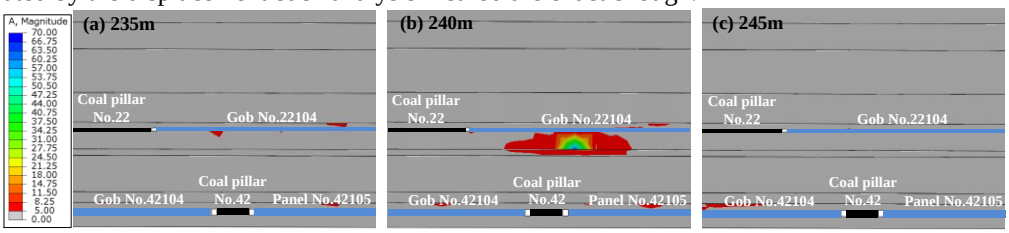

Fig. 10 The acceleration contour section maps at working face No.42105 when working face advances at (a) 235m, (b) 240m and (c) 245m.

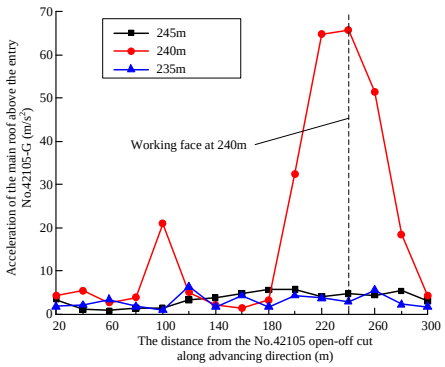

Fig. 11 The acceleration distribution along with the mining advancing direction of working face No.42105 in the main roof of coal seam No.42 above the entry No.42105-G.

4.3 The coal pillar energy release characteristics

Fig. 12 shows the strain energy density variation before and after the roof shock when working face No.42105 is advancing at 240 m. The location of the peak strain energy density in coal pillar No. 42 occurs behind the working face No.42105 due to the high mining-induced stress in this barrier coal pillar. Before roof

shock, the peak values of strain energy density in coal pillar No. 42 accumulates to an extremely high level of 1522 kJ/m^3. After roof shock, it decreases to 1341 kJ/m^3, indicating that the strain energy accumulated in the coal pillar is released. Moreover, it is a remarkable fact that the red zone of high strain energy density in Fig. 12 changes from continuity (A zone in Fig. 12(a)) to discontinuity (B zone in Fig. 12(b)), which strongly demonstrates that the strain energy in coal pillar No. 42 is released during roof shock.

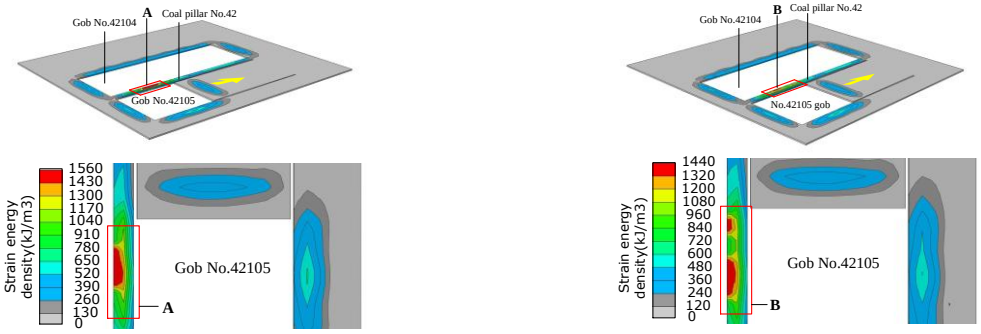

(a) (b)

Fig. 12 The strain energy density variation when working face No.42105 is advancing at 240m;(a) before roof shock; (b) after roof shock.

The peak strain energy density in coal pillar No. 42 with working face No.42105 advancing is shown in Fig. 13. The strain energy density data in Fig. 13 are picked in the beginning of each numerical mining cycle. At the beginning of mining, the peak strain energy density in coal pillar No. 42 is about 300 kJ/m^3, and it increases with the mining process until it reaches the maximum value of 1467 kJ/m^3 at 240 m. Then it reduces by 34.36% rapidly from 1467 kJ/m^3 at 240m to 963 kJ/m^3 at 250 m, implying the coal pillar experiences a sudden energy release. After 250 m, the peak strain energy density goes up and down slightly around an average value of 1138 kJ/m^3, and does not reappear sharp rise and fall, which suggests that the strain energy stored in coal pillar No. 42 tends to a stable state after 250 m. The above results indicate that the sudden drop of peak strain energy density in coal pillar can be an indicator for confirming a coal pillar burst accident, and is strongly relevant to the entry roof shock event. The continuous accumulation of strain energy density in barrier coal pillar is an effective omen and a risk index of roof shock in longwall coal mining process.

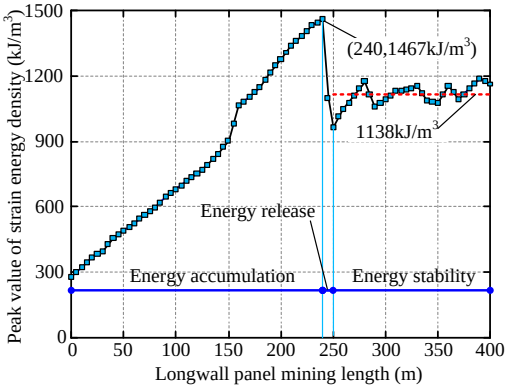

Fig. 13 The peak strain energy density variation with the mining process

4.4 The mining-induced stress evolution characteristics

The mining-induced stress evolution is useful to predict the fracture distance of the main key hard rock layer. The observation path of mining-induced stress is set in the middle of the observed panel along the working face advancing direction. In each numerical mining cycle for panels No. 22104 and No. 42105, the maximum mining-induced stress on the observation path and the vertical stress at the gob center are recorded, as shown in Fig. 14. With working face No. 22104 advancing, the maximum mining-induced stress on the observation path fluctuates periodically. It is generally assumed that these periodic peaks around or above 24 MPa in Fig. 14(a) are caused by the periodic breaks of the main key hard rock layer above the mined coal seam. Therefore, it can be speculated that the first fracture interval of the main key hard rock is about 180 m, and its periodic fracture interval is about 100 m. The in situ vertical stress of coal seam No. 22 is about 8 MPa according to its depth of 324.14 m, so the mining-induced stress concentration factor during panel No. 22104

mining is from 1.78 to 3.23.

Comparing Fig. 14(a) and (b), it is notable that the maximum mining-induced stress variations of panels No. 22104 and No. 42105 are significantly different as a result of the different mining conditions. The panel No. 22104 is mined under intact rock layer, whereas the panel No. 42105 is extracted under the gobs formed in No. 22 coal seam. When mining in panel No. 22104, the maximum mining-induced stress rises and drops sharply around the peaks. However, with working face No. 42105 advancing, the maximum mining-induced stress goes up gradually and declines rapidly. The in situ vertical stress of coal seam No. 42 is about 9.68 MPa according to its depth of 391.97 m, and it can be calculated that the maximum mining-induced stress concentration factor is from 1.65 to 2.56. Result suggests that the variation intensity of mining-induced stress in No. 42105 panel is more mitigatory relatively compared to that in panel No. 22104, as the rock layers above the coal seam No. 22 had fractured due to the mining activities in panel No. 22104. Moreover, when mining in panel No. 42105, the stress variation period is between 80 and 100 m, indirectly proving the fractured main key rock layer is reactivated periodically induced by mining in panel No. 42015. When working face No. 42105 is advancing at 240 m, the maximum mining-induced stress reaches the highest value, indicating the fractured main key hard layer slips down and may causes an impact onto the coal pillar No. 42.

The distance from the gob center to the open-off cut is a half of the distance from working face to the open-off cut. That is, if the gob center is at 80 m, the working face is advancing at 160 m. According to Fig. 14(c) and (d), the vertical stress at gob center gradually increases to the in situ vertical stress as a result of gob compaction with working face advancing. The vertical stress at gob No. 22104 center stabilizes around 8 MPa after working face No. 22104 advances at 180 m, and the vertical stress at gob No. 42105 center gradually reaches 9.68 MPa after working face No. 42105 advances at 160 m. The complete compaction of gob No. 42105 occurs when the main key hard strata breaks and slips down according to Fig. 14(b). In summary, the roof shock of entry No.42105-G when panel No. 42105 advances at 240 m is closely related to the slip of the fractured main key hard strata.

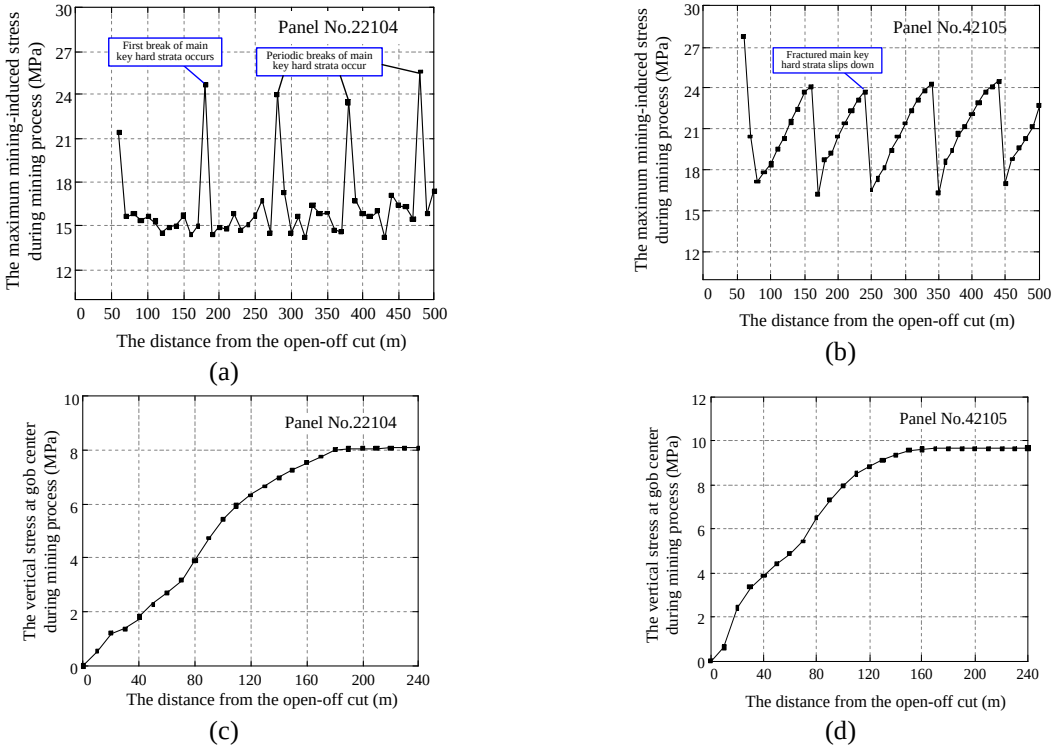

Fig. 14 The evolutions of maximum mining-induced stress and the vertical stress at gob center during mining process; (a) and (c) panel No. 22104; (b) and (d) panel No. 42105

5. 5 Mechanism of the entry roof shock

The evolution characteristics of the strata structure in Buertai coal mine can be inferred based on the overlying strata structure theory [39] and the numerical simulation results. In fact, the fractured strata structure induced by under-gob mining activities is very complex. To describe the entry roof shock mechanism more clearly, the strata structure is illustrated in a geological section view which is perpendicular to the mining advancing direction.

As shown in Fig. 15, according to the overlying strata structure theory, after the longwall panel on both

sides of the coal pillar is mined, a V-shaped strata structure is formed above the barrier coal pillar which is between the two gobs. The length of the rock beam in the V-shaped strata structure gradually increases with its vertical distance from the coal pillar. Obviously, the coal pillar is subjected to high pressure originating from the V-shaped strata structure and stores lots of strain energy.

In the under-gob mining situation of panel No. 42105 in Buertai coal mine, the V-shaped structure evolution is plotted in Fig. 15(a)-(c). From Fig. 15, a V-shaped strata structure above the coal pillar No. 22 is formed first, and then a series of stable and balanced rock beam chains are developed after panels No. 22103, No. 22104 and No. 22105 are extracted. When mining in panel No. 42105, the balance states of those overlying rock beam chains above coal seam No. 22 are broken. Especially, affected by the under-gob mining activity, the slip of the main key hard rock layer causes the V-shaped structure above coal pillar No. 22 to suddenly lose its support and fall over, which induces a dynamic impact on coal pillar No. 42. Consequently, subjecting to the static and dynamic coupling load, coal pillar No. 42 bursts and collapses with the entry roof shocking and subsiding, eventually causing the hydraulic single props destroyed (see Fig. 15(b) and (c)).

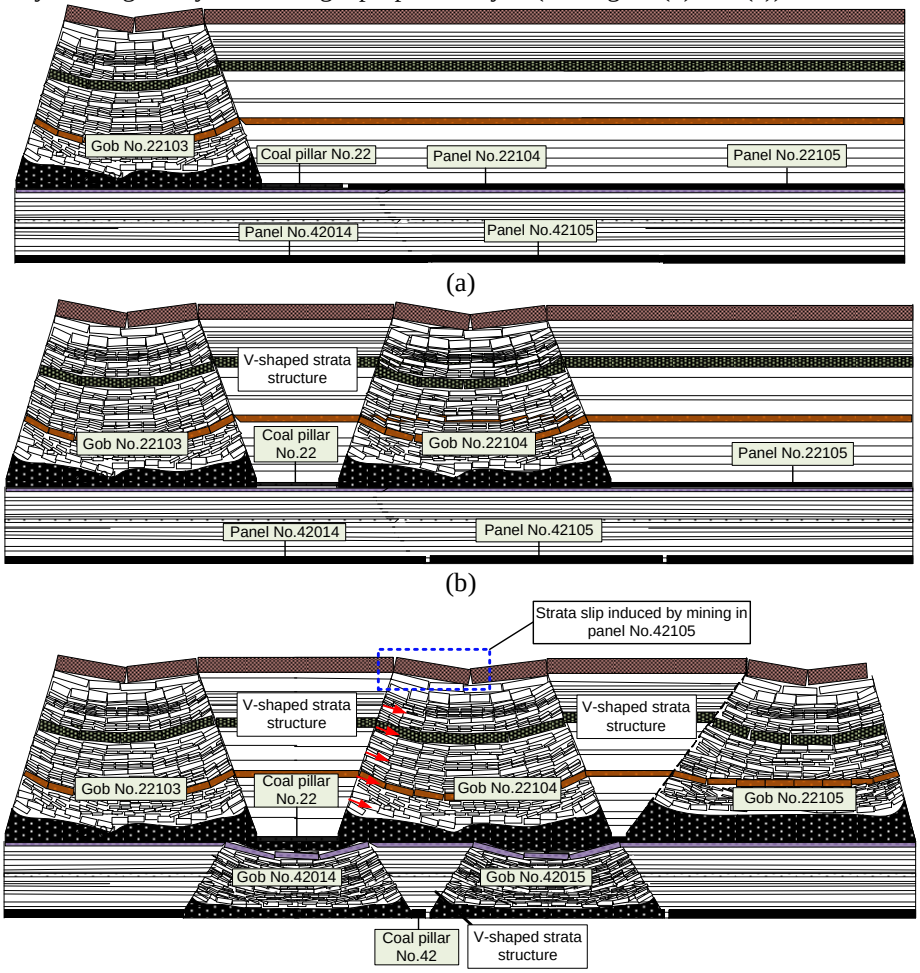

Fig. 15 The ground structure evolution in the under-gob mining situation in the geological section view perpendicular to the mining advancing direction; (a) after mining finished in panel No. 22103; (b) after mining finished in panel No. 22104; (c) after mining finished in panel No. 42105.

Before mining in coal seam No. 42, the V-shaped strata structure above coal pillar No.22 is intact in the mining advancing direction. When mining in panel No. 42104, this V-shaped structure periodically fractures due to its floor rock caving, forming several triangular-prism-shaped rock blocks, as shown in Fig. 16. When mining in panel No. 42105, those blocks of the V-shaped structure rotate and fall towards the V-shaped structure above coal pillar No.42 as the supporting forces on its right side are relieved. Therefore, the blocks fall of the V-shaped structure impacts onto the coal pillar No. 42. Under the combination of the dynamic loading and the high static loading, the bump in coal pillar No. 22 and the roof shock around entry No. 42105-G happened.

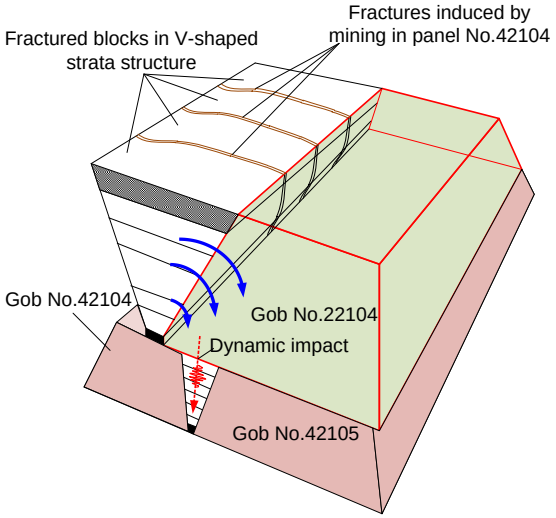

Fig. 16 Schematic of the dynamic impact induced by the rotation of the fractured blocks in V-shaped strata structure

6. Conclusions

In this study, the displacement back analysis method based on numerical modeling and field observations is conducted to investigate the entry roof shock accident and the coal pillar burst at longwall panel No. 42105 in Buertai coal mine. A back-analysis algorithm for determining the mechanical parameter values of rock mass is proposed and implemented with ABAQUS, and a static and dynamic coupling analysis approach is developed for longwall mining simulation based on the "Dynamic/Implicit" solving mode in ABAQUS. The least square objective function is adopted to optimize the input mechanical parameter values in displacement back analysis work. The variations of the acceleration distribution in main roof, the strain energy release process in barrier coal pillar and the mining-induced stress evolution during longwall mining process are obtained and analyzed. Based on the numerical simulation results and the overlying strata structure theory, the mechanism of the entry roof shock in the under-gob mining situation is inferred and explained. Specific conclusions are drawn as follows.

(1). The displacement back analysis method shows a good performance and feasibility to determine the rock mass mechanical parameter values for accurately modeling longwall mining process and the entry roof shock accident. According to the displacement back analysis results, the Mohr-coulomb strain softening model shows a good description in rock mass deformation behavior and the process of strain energy accumulation and release in coal pillar.

(2). The entry roof shock accident is very correlated with the strain energy release of the barrier coal pillar, indicating that the instantaneous instability of coal pillar triggers the entry roof shock accident. The continuous accumulation of strain energy in barrier coal pillar can be an effective omen and a risk index for predicting entry roof shock in longwall mining process.

(3). According to the numerical results of mining-induced stress evolution and the overlying strata structure theory, the coal pillar in lower coal seam is subjected to high pressure originating from the V-shaped strata structure and stores lots of strain energy. Affected by the under-gob mining activity, the fractured main key hard strata above the upper coal seam slip, causing the V-shaped strata blocks above the coal pillar in the upper coal seam to suddenly fall over and generating a dynamic impact onto the coal pillar in the lower coal seam. Subjected to the static-dynamic coupling load, the coal pillar in the under-gob panel bursts and collapses with the entry roof shocking and subsiding, eventually causing the hydraulic single props destroyed.

7. Acknowledgments

This work was financially supported by the National Natural Science Foundation of China (grant nos. 52204090), Fundamental Research Funds for the Universities of Henan Province (grant nos. NSFRF210334 and NSFRF210306).

8. Conflict of Interest

The authors declare that they have no known competing financial interests or personal relationships that could have appeared to influence the work reported in this paper.

References

[1]. He J, Dou LM, Gong SY, et al. Rock burst assessment and prediction by dynamic and static stress analysis based on micro-seismic monitoring. Int J Rock Mech Min Sci, 2017, 100(93):46-53. https://doi.org/10.1016/j.ijrmms.2017.01.005
[2]. Li T, Cai MF, Cai M. A review of mining-induced seismicity in China. Int J Rock Mech Min Sci, 2007, 44(8):1149–1171. https://doi.org/10.1016/j.ijrmms.2007.06.002
[3]. Mazaira A, Konicek P. Intense rockburst impacts in deep underground construction and their prevention. Can Geotech J, 2015, 52(10): 1426–1439. https://doi.org/10.1139/cgj-2014-0359
[4]. Mine Safety and Health Administration. Fatal Underground Coal Burst Accidents August 6 and 16, 2007. Report of investigation, 2007, CAI-2007-15-17.
[5]. Pechmann JC, Arabasz WJ, Pankow KL, et al. Seismological report on the 6 August 2007 Crandall Canyon Mine collapse in Utah. Seismol Res Lett, 2008, 79(5): 620–636. https://doi.org/10.1785/gssrl.79.5.620
[6]. Jiang YD, Zhao YX, Wang HW, et al. A review of mechanism and prevention technologies of coal bumps in China. J Rock Mech Geotech Eng, 2017, 9(1):180-194. https://doi.org/10.1016/j.jrmge.2016.05.008
[7]. Zhang CG, Canbulat I, Hebblewhite B, et al. Assessing coal burst phenomena in mining and insights into directions for future research. Int J Coal Geol, 2017, 179: 28-44. https://doi.org/10.1016/j.coal.2017.05.011
[8]. Pan JF, Mao DB, Lan H, et al. Study status and prospects of mine pressure bumping control technology in China. Coal Sci Technol (China), 2013, 41 (6): 21–25.
[9]. Yang ZQ, Dou LM, Liu C. Application of high-pressure water jet technology and the theory of rock burst control in roadways. Int J Min Sci Technol, 2016, 26(5): 929–35. https://doi.org/10.1016/j.ijmst.2016.05.037
[10]. Wang A, Yao QL, Li XH. Bolt fracture mechanism of roadway driven along gob in high street area caused by mining. J China Univ Min Technol (China), 2017, 46 (4):769–75.
[11]. Kabiesz J, Makówka J. Selected elements of rock burst state assessment in case studies from the Silesian hard coal mines. Min Sci Technol (China), 2009, 19(5):660–667. https://doi.org/10.1016/S1674-5264(09)60123-X
[12]. Cook, N. The seismic location of rockbursts. In: Proceedings 5th Symp Rock Mech Pergamon Press, 1963, 493–516.
[13]. Petukhov IM, Linkov AM. The theory of post-failure deformations and the problem of stability in rock mechanics. Int J Rock Mech Min Sci Geomech Abstr, 1979, 16(2):57–76. https://doi.org/10.1016/0148-9062(79)91444-X
[14]. Dou LM, He XQ. Prevention Theory and Technology of Rockburst. China University of Mining and Technology Press, 2001.
[15]. Jiang LS, Wang P, Zhang PP, et al. Numerical analysis of the effects induced by normal faults and dip angles on rock bursts. Comptes Rendus Mécanique, 2017, 345(10): 690-705. https://doi.org/10.1016/j.crme.2017.06.009
[16]. Zhang MT. Instability theory and mathematical model for coal/rock bursts. Chin J Rock Mech Eng, 1987, 6(3):197–204.
[17]. Jiang YD, Pan YS, Jiang FX, et al. State of the art review on mechanism and prevention of coal bumps in China. J China Coal Soc, 2014, 39(2): 205–213.
[18]. Jiang YD, Zhao YX. State of the art: investigation on mechanism, forecast and control of coal bumps in China. Chin J Rock Mech Eng, 2015, 34(11): 2188-2204.
[19]. He J. Research of mining dynamic loading effect and its induced rock burst in coal mine. Xuzhou: China University of Mining and Technology, 2013.
[20]. Dou LM, Mu ZL, Li ZL, et al. Research progress of monitoring, forecasting, and prevention of rockburst in underground coal mining in China. Int J Coal Sci Technol, 2014, 1(3): 278–288. https://xs.scihub.ltd/https://doi.org/10.1007/s40789-014-0044-z
[21]. Li ZL, Dou LM, Wang GF, et al. Risk evaluation of rock burst through theory of static and dynamic stresses superposition. J Cent South Univ, 2015, 22(2): 676-683.
[22]. Liu C, Li HM, Jiang DJ. Numerical simulation study on the relationship between mining heights and shield resistance in longwall panel. Int J Min Sci Technol, 2017, 27(2): 293-297. https://doi.org/10.1016/j.ijmst.2017.01.017
[23]. Hoek E. Strength of rock and rock masses. ISRM News Journal, 1994, 2(2): 4-16.
[24]. Hoek E, Kaiser PK, Bawden WF. Support of underground excavations in hard rock. Rotterdam: A.A. Balkema, 1995.
[25]. Hoek E, Marinos P, Benissi M. Applicability of the Geological Strength Index (GSI) classification for

very weak and sheared rock masses. The case of the Athens schist formation. B Eng Geol Environ, 1998, 57(2): 151-160.
[26]. Hoek E, Marinos P, Marinos V. Characterization and engineering properties of tectonically undisturbed but lithologically varied sedimentary rock masses. Int J Rock Mech Min Sci, 2005 42(2): 277-85.
[27]. Somodi G, Krupa Á, Kovács L et al. Comparison of different calculation methods of Geological Strength Index (GSI) in a specific underground construction site. Eng Geol, 2018, 243, 50-58.
[28]. [28] Hoek E, Brown ET. The Hoek–Brown failure criterion and GSI–2018 edition. J Rock Mech Geotech Eng, 2019, 11(3), 445-463.
[29]. Yu YZ, Zhang BY, Yuan HN. An intelligent displacement back-analysis method for earth-rockfill dams. Comput Geotech, 2007, 34(6), 423-434.
[30]. Xie HP, Chen ZD Fractal geometry and fracture of rock. Acta Mech Sinica-Prc, 1988, 4(3), 255-264.
[31]. Zinn-Justin J. Quantum field theory and critical phenomena. Clarendon Press, 1996.
[32]. Kong WX, Rui YQ, Dong BD. Determination of dilatancy angle for geomaterials under non-associated flow rule. Rock Soil Mech, 2009, 30(11): 3278-3282.
[33]. Abaqus V. 6.14 Documentation. Dassault Systemes Simulia Corporation, 2014.
[34]. Salamon M.D.G. Displacements and stresses induced by longwall mining in coal. In proceeding of the 7th Congress of the International Society for Rock Mechanics. Balkema, 1991, Rotterdam 1199–1202.
[35]. Pappas DM, Mark C. Behavior of Simulated Longwall Gob material (No. 9458). United States Department of the Interior- Bureau of mines, 1993.
[36]. Badr S, Mendoza R, Kieffer S, et al. Numerical Modeling of Longwalls in Deep Coal Mines, in: Proceeding of the 22nd International Conference on Ground Control in Mining. Morgantown, West Virginia 7, 2003.
[37]. Castro LA, Grabinsky MW, McCreath DR. Damage initiation through extension fracturing in a moderately jointed brittle shear rock mass. Int J Rock Mech Min Sci, 1997, 34(3-4):110-113.
[38]. Xie HP, Li LY, Peng RD, et al. Energy analysis and criteria for structural failure of rocks, J Rock Mech Geotech Eng,2009, 1(1): 11-20.
[39]. Jiang FX, Zhang XM, Yang SL, et al. Discussion on overlying strata spatial structures of longwall in coal mine. Chin J Rock Mech Eng, 2006, 25(5): 979-984.